Supplementary Information

Mapping the Energy Landscape of a Supramolecular System via Time-Resolved Asymmetric-Flow Field Flow Fractionation

Maria Kariuki,[a] Julia Y. Rho,[b] and Sébastien Perrier* [a, b, c]

a. Department of Chemistry, University of Warwick, Coventry CV4 7AL, UK

b. Warwick Medical School, University of Warwick, Coventry CV4 7AL, UK

c. Faculty of Pharmacy and Pharmaceutical Sciences, Monash University, Parkville, VIC 3052, Australia.

* Corresponding author: s.perrier@warwick.ac.uk

A. Supplementary Results

A.1 Standard Protocol

S1a).

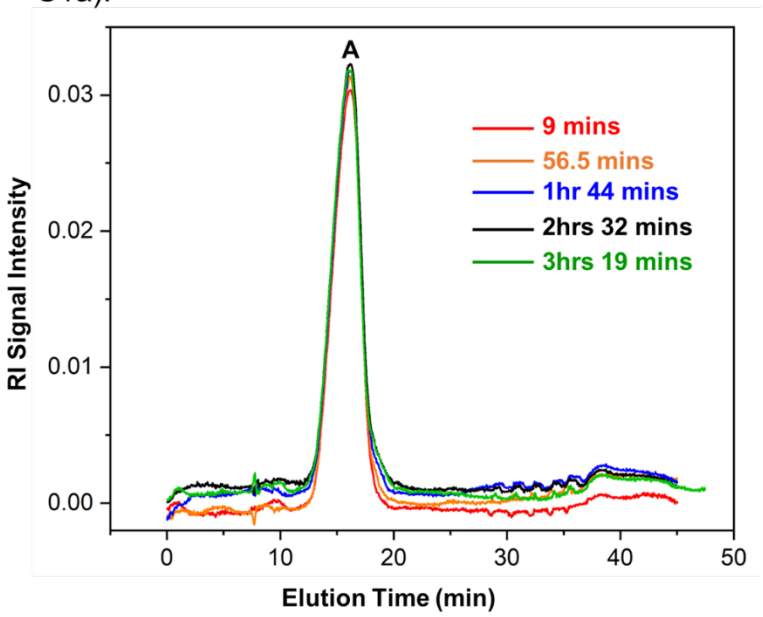

S1b).

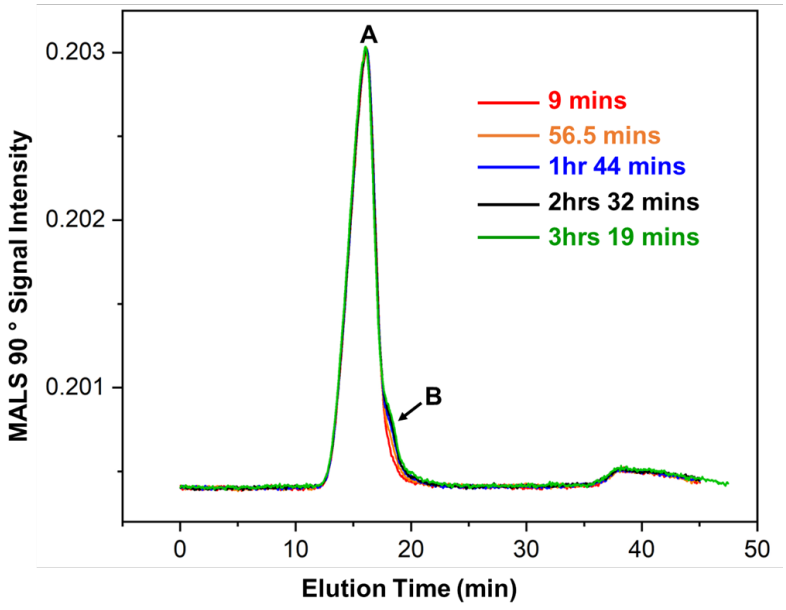

Figure S1 (a-b): Time-resolved AF_4-MALS-RI fractograms of the CP-[$p(BA)_5$-b-$p(DMA)_{45}$]$_2$ conjugate, collected via sequential runs during the first experiment. The first timepoint (9 mins) represents the time elapsed between sample preparation and the start of the run sequence.

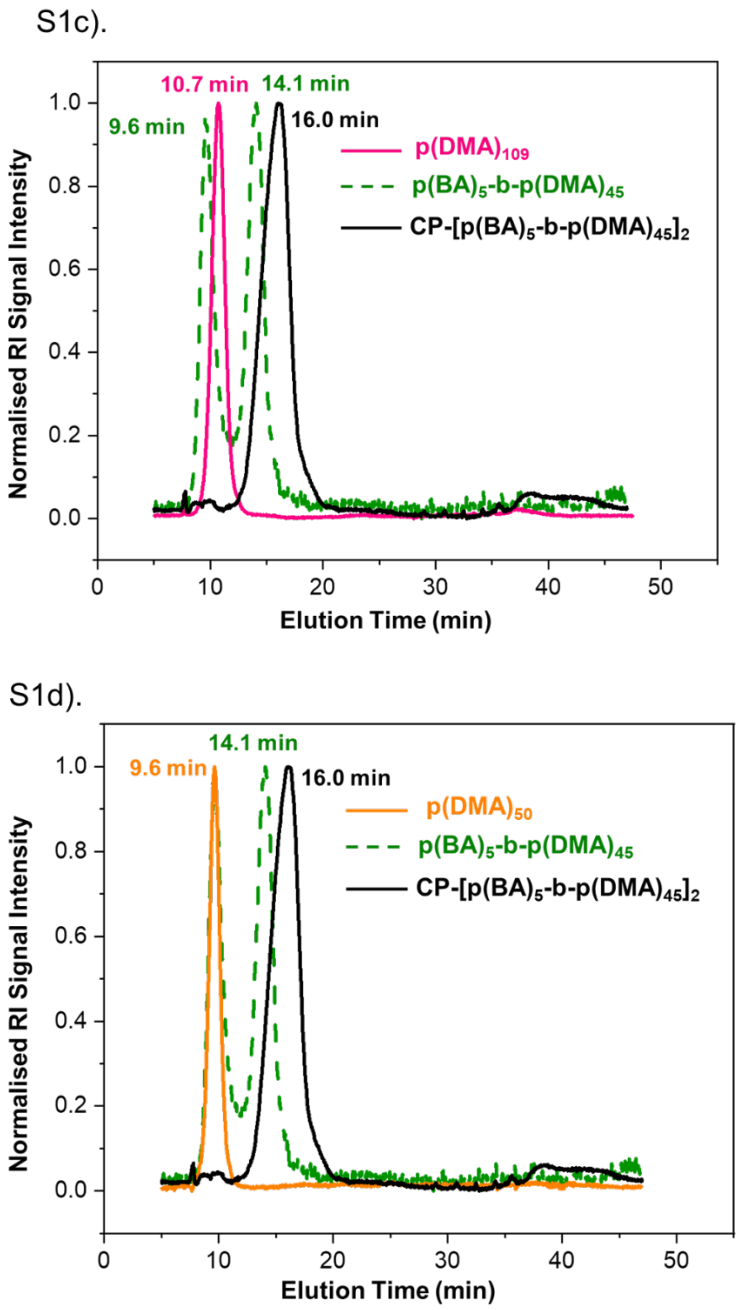

Figure S1 (c-d): Comparison of the conjugate (CP-[p(BA)$_5$-b-p(DMA)$_{45}$]$_2$) to its control, unconjugated polymers via their measured RI detector signals. The signal from the amphiphilic diblock copolymer confirms that the conjugate's measured populations do not correspond to micelles. This is verified by the differences in the peak elution times and distribution profiles. The control hydrophilic polymers confirm the absence of one-arm and two-arm conjugate unimers. pDMA$_{50}$ also identifies the unassembled amphiphilic diblock copolymers. NB: The kinetic timepoint of the example conjugate fractogram is 9 mins.

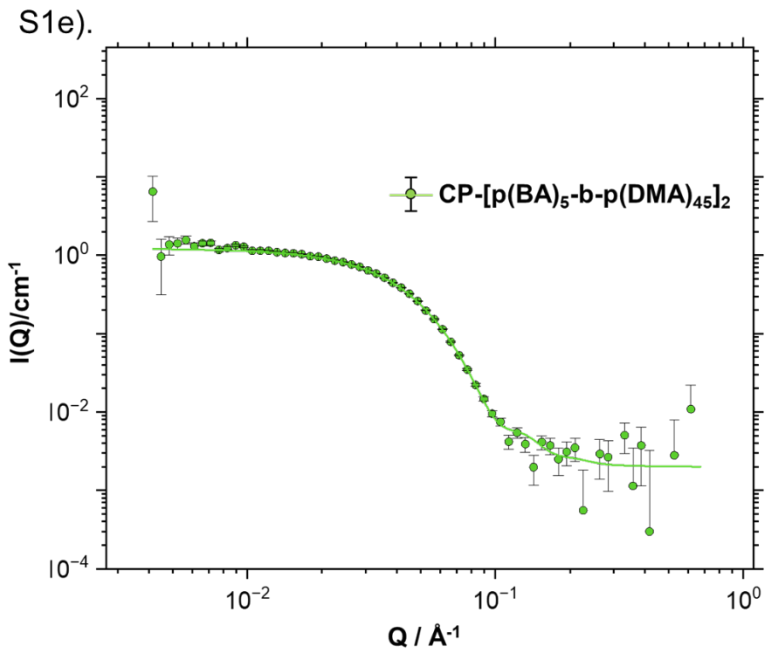

Figure S1 (e): SANS scattering profile of the conjugate in 95% D_2O and 5% d-DMSO, collected at 24 hours. A core-shell cylinder model provided the best fit with a low Chi^2 value. Experimental details are available in the referenced literature[18]

Table S1: Summary of the molecular weight limits and averages (UL, LL M_w, M_n) and aggregation number (N_{agg}) of the detected populations in Figure S1a-1b. NB: The shoulder peaks (B) observed from 1hr 44 mins had very low signal intensities hence calculations could not be performed.

[§] Kinetic Timepoint	Peak	*UL	*LL	*M_w	*M_n	[†]N_{agg}
9 mins	A	2.953×10^5	1.699×10^5	2.314×10^5	1.711×10^5	14←20→25
56 mins	A	2.971×10^5	1.762×10^5	2.343×10^5	2.233×10^5	15←20→25
1hr 44 mins	A	2.928×10^5	1.753×10^5	2.318×10^5	2.189×10^5	15←20→25
2 hrs 32 mins	A	2.970×10^5	1.778×10^5	2.338×10^5	2.218×10^5	15←20→25
3 hrs 19 mins	A	2.861×10^5	1.692×10^5	2.238×10^5	2.021×10^5	14←19→24

[§] Indicates the time elapsed between sample preparation and analysis. * Common units: Da or g mol^{-1}; Mw & M_n: weight- and number-average molecular weights; UL&LL: upper and lower molecular weight limits used as a measure of dispersity. The limits denote where 75% of the peak distribution lies within ±2 standard deviations (2σ) away from the mean (M_w).[38] [†] The N_{agg} range of the assemblies within the specified peak, calculated from the M_w (mean), UL (right, +2σ) and LL (left, -2σ); Formula = (MW value) ÷ theoretical MW of conjugate unimer (1.173×10^4).

A.2 Comparison Protocol

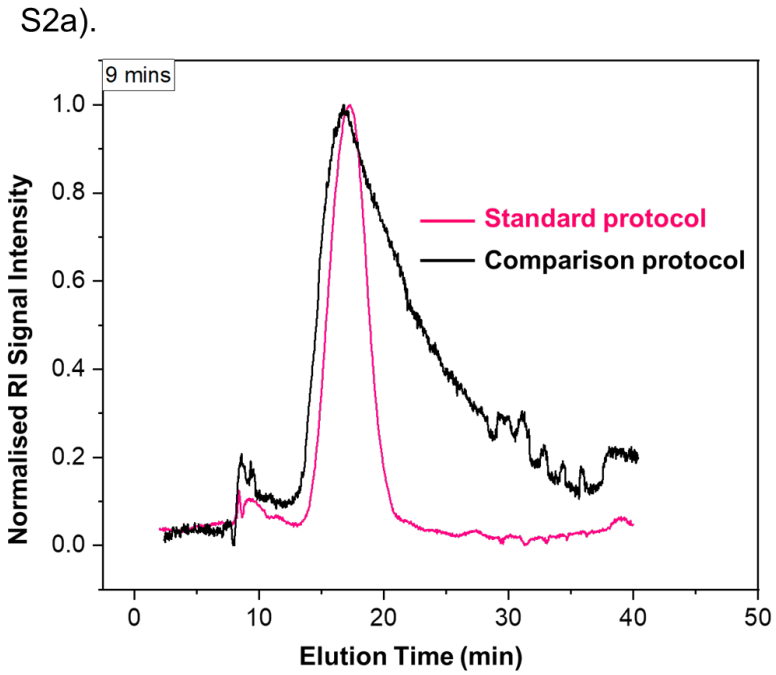

Figure S2. (a) Comparison of the conjugate fractograms collected at the first kinetic timepoint (9 mins) following preparation by both protocols. From their measured RI detector signals, the presence of single nanotubes in the distribution of the comparison protocol is supported.

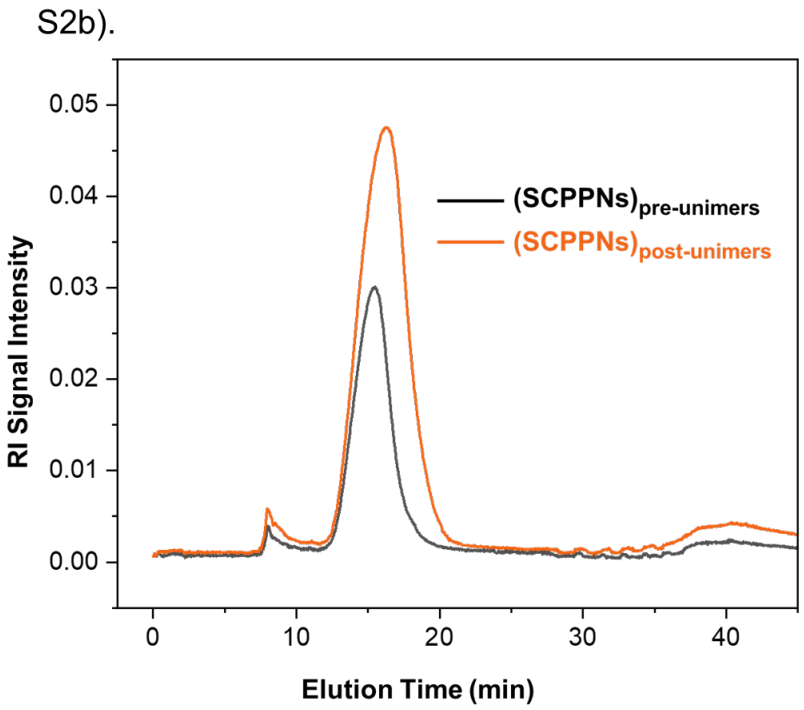

Figure S2. (b) Fractogram comparisons of the differences in the distribution of individual nanotubes following the addition of free unimers. An increase in the concentration of the SCPPNs is primarily noted as well as a slight broadening of their distribution, indicating growth of the nanotubes. See Table S2.

Table S2: Summary of the detected concentrations, molecular weight limits and averages (UL, LL M_w, M_n) and aggregation number (N_{agg}) of the individual nanotube populations in Figure S2b.

Distribution	Conc (mg/mL)	*UL	*LL	*M_w	*M_n	†N_{agg}
Pre-unimers	0.833	2.341 x 10^5	1.204 x 10^5	1.730 x 10^5	1.523 x 10^5	10←15→20
Post-unimers	1.685	2.432 x 10^5	1.267 x 10^5	1.793 x 10^5	1.623 x 10^5	11←15→21

* Common units: Da or g mol^{-1}; Mw & M_n: weight- and number-average molecular weights; UL&LL: upper and lower molecular weight limits used as a measure of dispersity. The limits denote where 75% of the peak distribution lies within ±2 standard deviations (2σ) away from the mean (M_w).[38] † The N_{agg} range of the assemblies within the specified peak, calculated from the M_w (mean), UL (right, +2σ) and LL (left, -2σ); Formula = (molecular weight value) ÷ theoretical molecular weight of conjugate unimer (1.173 x 10^4).

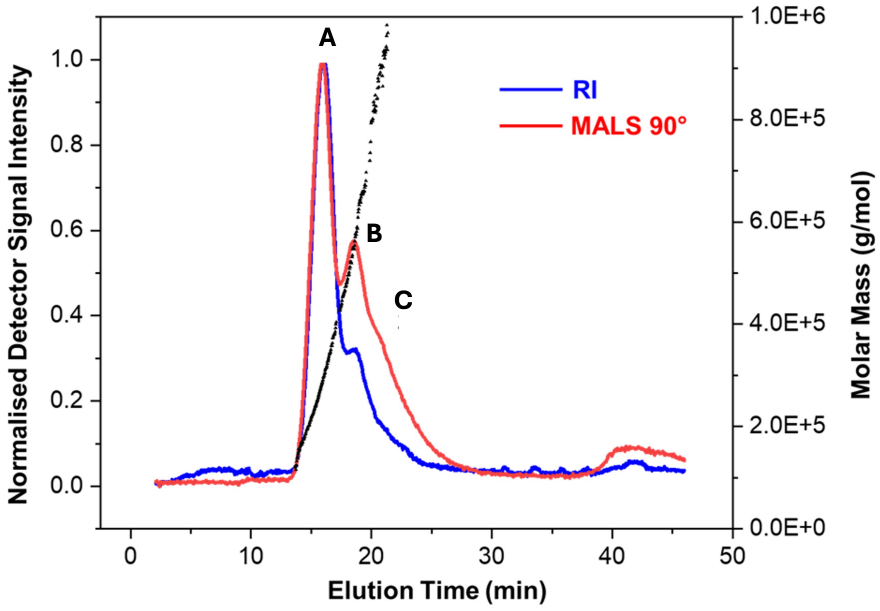

Figure S3. Time-resolved AF_4-MALS-RI fractograms of the amphiphilic conjugate (CP-[$p(BA)_5$-b-$p(DMA)_{45}]_2$) after one week. The blue and red traces are the RI and MALS detector signals, respectively. The overlaid black traces (right y-axis) are the molecular weight values for each elution fraction.

B. Experimental Protocols

B.1 AF_4 Instrumentation

All measurements were conducted using PostNova Analytics AF2000 multi-flow system (Malvern, UK) with a PN5300 injection autosampler. To allow for a multi-detection setup, XXdifferential refractive index (RI) PN3150 detector and multi-angle light scattering (MALS) PN3621 detector were connected online to the system. Light

scattering was measured using a 50-mW laser operating at a wavelength of 532 nm (green), and the resulting signals were detected from 21 observation angles ranging between 7 to 164 °. Sample separation was conducted within a channel (335 x 60 x 40 mm) containing a trapezoidal polytetrafluoroethylene spacer (PTFE, 350 µm thickness) and a semipermeable regenerated cellulose (RC) membrane with a 10 kDa nominal molecular weight cutoff. Note the channel and all its components were also provided by PostNova Analytics (Malvern, UK). Data acquisition and processing were controlled through the PostNova AF2000 software version 2105.

B.2 Detector Calibration & System Performance

Prior to the measurements, calibration of the detectors was performed according to the manufacturer manual to determine the detector constants. Lyophilized Bovine Albumin Serum (BSA, 1 mg mL^{-1}) prepared in 0.9 % NaCl aqueous solvent was used to calibrate the RI detector. The MALS detector was also calibrated using a BSA solution (5 mg mL^{-1}), and the scattering angles were normalised against a polystyrene sulfonate sodium salt solution (PSS, 67 kDa, $Đ \leq 1.2$, 10 mg mL-1) or a latex mixture: 3000 Series NIST certified polystyrene nano sphere particle size standards with nominal diameters (nm) of 23 ± 2 (0.4 mg mL-1), 61 ± 4 (0.04 mg mL-1) and 122 ± 3 (0.008 mg mL-1). PSS normalisation was performed for soluble macromolecules and the standard solution was prepared using 0.9% NaCl solvent. Latex normalisation was conducted for particles and the mixture was prepared using a 0.2% NovaChem surfactant solution: a mixture of non-ionic and ionic detergents. Lastly, the calibration and separation performance of the AF_4 channel was evaluated by fractionating BSA (1 mg mL^{-1}). System performance is confirmed by the good resolution of its monomer (66 kDa), dimer and trimer peaks and calibration is validated by obtaining the correct molecular weight values of the peaks.

B.3 Eluent Preparation

The aqueous solvent used for sample preparation and measurement was prepared by dissolving sodium azide (NaN_3, 0.02%) and sodium chloride (NaCl, 0.1M) in HPLC-grade water. NaCl was added to prevent nonspecific sample-membrane electrostatic interactions and the NaN_3 prevents bacterial contamination.[52] Before use, the eluent was vacuum filtered through 0.1 µM aqueous compatible filters to remove any impurities that would interfere with the light scattering signals, particularly at low angles.[30] The calibration solvent consisting of 0.9% NaCl was prepared similarly, i.e. dissolution of

the salt in HPLC grade water followed by eluent filtration, whilst the 0.2% NovaChem surfactant solution was prepared by filtering the HPLC grade water before dissolving the surfactant. Note dissolution in all cases was aided by gentle stirring and filtration was conducted using PTFE filters purchased from PostNova Analytics.

B.4 Method Development

The method conditions used to analyse the samples in this study are summarised below in **Table S3.**

Table S3: Programmed AF_4 experimental conditions used in this study. Note the channel outlet flow (detector-flow) rate was held constant at 0.5 mL/min during each analysis.

Step	Conditions
Injection + Focus	Injection volume: 50 µL Injection time: 6 mins Injection flow: 0.2 mL/min Cross flow (CF): 1.75 mL/min Focus flow: 2.05 mL/min Transition time: 1 min
Elution (CF Programming)	Step 1 (20 mins): CF held constant at 1.75 mL/min Step 2 (10 mins): CF decayed linearly from 1.75 mL/min to 0.07 mL/min Step 3 (10 mins): CF held constant at 0.07 mL/min
Rinse	Before the start of the next run, a brief rinse was performed at a channel (TIP) flow rate of 0.1mL/min for 30 seconds.

B.5 Determination of the Molecular Weight Averages and Concentration

The molecular weight distribution is defined by a series of volume slices (*i*) containing a specific concentration of molecules presumed to be similar in their molecular weights.[30, 53-55] The concentration of the molecules in each slice is determined from the refractive index detector signal according to equation (1a). In contrast, their molecular weight is determined using the Zimm formalism equation and based on the assumption that the polydispersity of the molecules is negligible. Briefly, the Zimm formalism relates the measured light scattering signal intensity to the molecular weight and concentration of the molecules, equation (1b).[30, 53-55] The data obtained from each slice is then used to calculate the molecular weight averages of the distribution, namely the weight- (M_w) and number-average (M_n), see equations (1c-1d).[30, 53-55]

$$C_i = \frac{\eta_0 \times RI_i}{K_{RI} \times \frac{\partial n}{\partial c}} \qquad (1a)$$

Where RI is the measured refractive index signal, K_{RI} is the calibration constant and η_0 is the refractive index of the detector cell reference solvent. The subscript *i* indicates the elution volume slice.

$$\left(\frac{1}{MW_i}\right) = \frac{KC}{R_\theta} - 2A_2C_i \quad (1b)$$

Where K is an optical constant that is dependent on the $\partial n/\partial c$ of the matrix; C is the concentration; MW is molecular weight; R_θ is the excess Rayleigh ratio of the solution (ratio of the scattered and incident light intensity) and A_2 is the second virial coefficient which is a measure of sample-sample interaction.

$$M_w = \frac{\Sigma C_i MW_i}{\Sigma C_i} \quad (1c)$$

$$M_n = \frac{\Sigma C_i}{\Sigma(\frac{C_i}{MW_i})} \quad (1d)$$

Note the sum of C_i ($\sum C_i$) is the total concentration of the distribution.

B.6 Estimation of the $\partial n/\partial c$

B.6.1 Measurement Protocol

The $\partial n/\partial c$ value of the conjugate was estimated online from the RI detector signals of its control amphiphilic diblock copolymer. Polymer solutions of known concentrations were prepared using the aqueous solvent and were measured by AF_4 without applying a separation cross-flow field to fulfil the assumption of 100% recovery. Any inconsistency in the detected cumulative concentration was therefore related back to an erroneous $\partial n/\partial c$ value and the $\partial n/\partial c$ was adjusted until the target concentration was met. At least three consistent measurements were collected per solution and the mean $\partial n/\partial c$ value obtained was 0.2105 ± 0.0027 mL/g (at 25°C, λ = IR-UV range).

Note that an online approach was implemented as it is fast, straightforward and requires the preparation of fewer samples in comparison to batch analyses.[30, 55] In addition, the group has validated the accuracy of this approach using common polymer standards whose $\partial n/\partial c$ values are available in the literature.

B.6.2 Assumptions & Justification

The unconjugated polymer was used to estimate the $\partial n/\partial c$ due to the much lower cyclic peptide yield attainable during synthesis (mg) and the higher synthesis costs. It was postulated that the $\partial n/\partial c$ value of the polymer and the conjugate are similar since the conjugate structure primarily compromises the attached polymers, i.e. by weight fraction. It was also assumed, in line with theory, that the $\partial n/\partial c$ value would be valid

for both unimers and nanotube assemblies as the $\partial n/\partial c$ vary negligibly with increasing molecular weight (from $\geq 10^3$ Da).[56-58] Lastly, it was theorised that the obtained $\partial n/\partial c$ value proportionately accounted for the contributions of both copolymer blocks.[56, 57] This assumption was necessary as the $\partial n/\partial c$ of the hydrophobic block could not be individually determined in the aqueous solution used for analysis. Regarding the preparation of the polymer solutions, it is worth noting that DMSO was not added as it would have falsified the refractive index (RI) readings. This is because when conducting $\partial n/\partial c$ measurements, the sample and measurement eluent must match so that changes in the RI readings can be solely accounted to the sample at a specific concentration.[55] Nonetheless, it was confirmed that the polymer behaviour in the 5% DMSO and 0% DMSO solutions was the same.[18]

B.7 Estimation of the Dispersity (Upper and Lower Limits)

Dispersity within a distribution was measured by standard deviation (σ), which defines the variation of points away from the average value.[38, 59, 60] In this study, the deviation is determined based on an empirical probability rule that applies to any distribution type.[38] Under this rule, at least 75% of the distribution values fall within two standard deviations (±2σ) away from the mean.[38] The upper and lower molecular weight limits corresponding to a 75% confidence interval were determined from each detected peak's cumulative molecular weight distribution plot.[30] Note the relative standard deviation ([σ/mean]*100) was used to compare the dispersity between different populations or samples.

References

1. Korevaar, P. A.; Newcomb, C. J.; Meijer, E. W.; Stupp, S. I., Pathway Selection in Peptide Amphiphile Assembly. *Journal of the American Chemical Society* **2014,** *136* (24), 8540-8543.

2. Ogi, S.; Sugiyasu, K.; Manna, S.; Samitsu, S.; Takeuchi, M., Living supramolecular polymerization realized through a biomimetic approach. *Nature Chemistry* **2014,** *6* (3), 188-195.

3. Ogi, S.; Stepanenko, V.; Sugiyasu, K.; Takeuchi, M.; Würthner, F., Mechanism of Self-Assembly Process and Seeded Supramolecular Polymerization of Perylene Bisimide Organogelator. *Journal of the American Chemical Society* **2015,** *137* (9), 3300-3307.

4. Korevaar, P. A.; George, S. J.; Markvoort, A. J.; Smulders, M. M. J.; Hilbers, P. A. J.; Schenning, A. P. H. J.; De Greef, T. F. A.; Meijer, E. W., Pathway complexity in supramolecular polymerization. *Nature* **2012,** *481* (7382), 492-496.

5. Korevaar, P. A.; de Greef, T. F. A.; Meijer, E. W., Pathway Complexity in π-Conjugated Materials. *Chemistry of Materials* **2014,** *26* (1), 576-586.

6. Tantakitti, F.; Boekhoven, J.; Wang, X.; Kazantsev, R. V.; Yu, T.; Li, J.; Zhuang, E.; Zandi, R.; Ortony, J. H.; Newcomb, C. J.; Palmer, L. C.; Shekhawat, G. S.; de la Cruz, M. O.; Schatz, G. C.; Stupp, S. I., Energy landscapes and functions of supramolecular systems. *Nature Materials* **2016,** *15* (4), 469-476.

7. Zhang, K.; Yeung, M. C.-L.; Leung, S. Y.-L.; Yam, V. W.-W., Energy Landscape in Supramolecular Coassembly of Platinum(II) Complexes and Polymers: Morphological Diversity, Transformation, and Dilution Stability of Nanostructures. *Journal of the American Chemical Society* **2018,** *140* (30), 9594-9605.

8. Hashim, P. K.; Bergueiro, J.; Meijer, E. W.; Aida, T., Supramolecular Polymerization: A Conceptual Expansion for Innovative Materials. *Progress in Polymer Science* **2020,** *105*, 101250.

9. Matern, J.; Dorca, Y.; Sánchez, L.; Fernández, G., Revising Complex Supramolecular Polymerization under Kinetic and Thermodynamic Control. *Angewandte Chemie International Edition* **2019,** *58* (47), 16730-16740.

10. Grötsch, R. K.; Boekhoven, J., Unique properties of supramolecular biomaterials through nonequilibrium self-assembly. In *Self-assembling Biomaterials*, Azevedo, H. S.; da Silva, R. M. P., Eds. Woodhead Publishing: 2018; pp 235-250.

11. Sorrenti, A.; Leira-Iglesias, J.; Markvoort, A. J.; de Greef, T. F. A.; Hermans, T. M., Non-equilibrium supramolecular polymerization. *Chemical Society Reviews* **2017,** *46* (18), 5476-5490.

12. Dhiman, S.; George, S. J., Temporally Controlled Supramolecular Polymerization. *Bulletin of the Chemical Society of Japan* **2018,** *91* (4), 687-699.

13. De Greef, T. F. A.; Smulders, M. M. J.; Wolffs, M.; Schenning, A. P. H. J.; Sijbesma, R. P.; Meijer, E. W., Supramolecular Polymerization. *Chemical Reviews* **2009,** *109* (11), 5687-5754.

14. Hartlieb, M.; Mansfield, E. D. H.; Perrier, S., A guide to supramolecular polymerizations. *Polymer Chemistry* **2020,** *11* (6), 1083-1110.

15. Ghadiri, M. R.; Granja, J. R.; Milligan, R. A.; McRee, D. E.; Khazanovich, N., Self-assembling organic nanotubes based on a cyclic peptide architecture. *Nature* **1993,** 366, (6453), 324-327.

16. Rho, J. Y.; Perrier, S., 100th Anniversary of Macromolecular Science Viewpoint: User's Guide to Supramolecular Peptide–Polymer Conjugates. *ACS Macro Letters* **2021,** *10* (2), 258-271.

17. Song, Q.; Cheng, Z.; Kariuki, M.; Hall, S. C. L.; Hill, S. K.; Rho, J. Y.; Perrier, S., Molecular Self-Assembly and Supramolecular Chemistry of Cyclic Peptides. *Chemical Reviews* **2021**.

18. Yang, L.; Tan, X.; Wang, Z.; Zhang, X., Supramolecular Polymers: Historical Development, Preparation, Characterization, and Functions. *Chemical Reviews* **2015,** *115* (15), 7196-7239.

19. Liu, Y.; Wang, Z.; Zhang, X., Characterization of supramolecular polymers. *Chemical Society Reviews* **2012,** *41* (18), 5922-5932.

20. Modena, M. M.; Rühle, B.; Burg, T. P.; Wuttke, S., Nanoparticle Characterization: What to Measure? *Advanced Materials* **2019,** *31* (32), 1901556.

21. Kariuki, M.; Rho, J. R.; Hall, S. C. L.; Perrier, S. Investigating the Impact of Hydrophobic Polymer Segments on the Self-Assembly Behavior of Supramolecular Cyclic Peptide Systems via Asymmetric-Flow Field Flow Fractionation, *Macromolecules* **2023** *56* (17), 6618-6632.

22. Rho, J. Y.; Cox, H.; Mansfield, E. D. H.; Ellacott, S. H.; Peltier, R.; Brendel, J. C.; Hartlieb, M.; Waigh, T. A.; Perrier, S., Dual self-assembly of supramolecular peptide nanotubes to provide stabilisation in water. *Nature Communications* **2019,** *10* (1), 4708.

23. Abraham, M. H.; Grellier, P. L.; Prior, D. V.; Morris, J. J.; Taylor, P. J., Hydrogen bonding. Part 10. A scale of solute hydrogen-bond basicity using log K values for complexation in tetrachloromethane. *Journal of the Chemical Society, Perkin Transactions 2* **1990,** (4), 521-529.

24. Rho, J. Y.; Brendel, J. C.; MacFarlane, L. R.; Mansfield, E. D. H.; Peltier, R.; Rogers, S.; Hartlieb, M.; Perrier, S., Probing the Dynamic Nature of Self-Assembling Cyclic Peptide–Polymer Nanotubes in Solution and in Mammalian Cells. *Advanced Functional Materials* **2018,** *28* (24), 1704569.

25. Hartgerink, J. D.; Granja, J. R.; Milligan, R. A.; Ghadiri, M. R., Self-Assembling Peptide Nanotubes. *Journal of the American Chemical Society* **1996,** *118* (1), 43-50.

26. Tomasic, L.; Lorenzi, G. P., Some Cyclic Oligopeptide with S2n Symmetry. *Helvetica Chimica Acta* **1987,** *70* (4), 1012-1016.

27. Ghadiri, M. R.; Granja Jr Fau - Milligan, R. A.; Milligan Ra Fau - McRee, D. E.; McRee De Fau - Khazanovich, N.; Khazanovich, N., Self-assembling organic nanotubes based on a cyclic peptide architecture. *Nature* **1993,** *366*, 324-327.

28. Schimpf, M. E.; Caldwell, K.; Giddings, J. C., *Field flow fractionation handbook*. Wiley-Interscience: New York, 2000.

29. Lespes, G.; Gigault, J.; Battu, S., Field Flow Fractionation. *Analytical Separation Science* **2015,** *4*, 1143-1176.

30. Podzimek, S., *Light Scattering, Size Exclusion Chromatography and Asymmetric Flow Field Flow Fractionation: Powerful Tools for the Characterization of Polymers, Proteins and Nanoparticles*. John Wiley & Sons: New Jersey, 2011.

31. Podzimek, S., Asymmetric Flow Field Flow Fractionation. In *Encyclopedia of Analytical Chemistry*, John Wiley & Sons, Ltd: 2012.

32. Mansfield, E. D. H.; Hartlieb, M.; Catrouillet, S.; Rho, J. Y.; Larnaudie, S. C.; Rogers, S. E.; Sanchis, J.; Brendel, J. C.; Perrier, S., Systematic study of the structural parameters affecting the self-assembly of cyclic peptide–poly(ethylene glycol) conjugates. *Soft Matter* **2018,** *14* (30), 6320-6326.

33. Couet, J.; Samuel, J. D. J. S.; Kopyshev, A.; Santer, S.; Biesalski, M., Peptide–Polymer Hybrid Nanotubes. *Angewandte Chemie International Edition* **2005,** *44* (21), 3297-3301.

34. Couet, J.; Biesalski, M., Polymer-Wrapped Peptide Nanotubes: Peptide-Grafted Polymer Mass Impacts Length and Diameter. *Small* **2008,** *4* (7), 1008-1016.

35. Greenfield, N. J., Analysis of the kinetics of folding of proteins and peptides using circular dichroism. **2006,** *6*, 2891-2899.

36. Piskulich, Z. A.; Mesele, O. O.; Thompson, W. H., Activation Energies and Beyond. *The Journal of Physical Chemistry A* **2019,** *123* (33), 7185-7194.

37. Vyazovkin, S., Activation Energies and Temperature Dependencies of the Rates of Crystallization and Melting of Polymers. . *Polymer Chemistry* **2020,** *12* (5), 1070.

38. Harrisson, S., The downside of dispersity: why the standard deviation is a better measure of dispersion in precision polymerization. *Polymer Chemistry* **2018,** *9* (12), 1366-1370.

39. Haynie, D. T., *Biological Thermodynamics*. 2 ed.; Cambridge University Press: Cambridge, 2008.

40. Schauperl, M.; Podewitz, M.; Waldner, B. J.; Liedl, K. R., Enthalpic and Entropic Contributions to Hydrophobicity. *Journal of Chemical Theory and Computation* **2016,** *12* (9), 4600-4610.

41. Rayment, I., Protein Structure. In *Encyclopedia of Physical Science and Technology (Third Edition)*, Meyers, R. A., Ed. Academic Press: New York, 2003; pp 191-218.

42. Cramer, J.; Jiang, X.; Schönemann, W.; Silbermann, M.; Zihlmann, P.; Siegrist, S.; Fiege, B.; Jakob, R. P.; Rabbani, S.; Maier, T.; Ernst, B., Enhancing the enthalpic contribution of hydrogen bonds by solvent shielding. *RSC Chemical Biology* **2020,** *1* (4), 281-287.

43. Grdadolnik, J.; Merzel, F.; Avbelj, F., Origin of hydrophobicity and enhanced water hydrogen bond strength near purely hydrophobic solutes. *Proceedings of the National Academy of Sciences* **2017,** *114* (2), 322-327.

44. Chapman, R.; Koh, M. L.; Warr, G. G.; Jolliffe, K. A.; Perrier, S., Structure elucidation and control of cyclic peptide-derived nanotube assemblies in solution. *Chemical Science* **2013,** *4* (6), 2581-2589.

45. Clark, T. D.; Buriak, J. M.; Kobayashi, K.; Isler, M. P.; McRee, D. E.; Ghadiri, M. R., Cylindrical β-Sheet Peptide Assemblies. *Journal of the American Chemical Society* **1998,** *120* (35), 8949-8962.

46. Kobayashi, K.; Granja, J. R.; Ghadiri, M. R., Beta-Sheet Peptide Architecture: Measuring the Relative Stability of Parallel vs. Antiparallel Beta-Sheets. *Angewandte Chemie International Edition in English* **1995,** *34* (1), 95-97.

47. Ghadiri, M. R.; Kobayashi, K.; Granja, J. R.; Chadha, R. K.; McRee, D. E., The Structural and Thermodynamic Basis for the Formation of Self-Assembled Peptide Nanotubes. *Angewandte Chemie International Edition in English* **1995,** *34* (1), 93-95.

48. Larnaudie, S. C.; Sanchis, J.; Nguyen, T.-H.; Peltier, R.; Catrouillet, S.; Brendel, J. C.; Porter, C. J. H.; Jolliffe, K. A.; Perrier, S., Cyclic peptide-poly(HPMA) nanotubes as drug delivery vectors: In vitro assessment, pharmacokinetics and biodistribution. *Biomaterials* **2018,** *178*, 570-582.

49. Torchilin, V., Tumor delivery of macromolecular drugs based on the EPR effect. *Advanced Drug Delivery Reviews* **2011,** *63* (3), 131-135.

50. Ahmad, Z.; Shah, A.; Siddiq, M.; Kraatz, H.-B., Polymeric micelles as drug delivery vehicles. *RSC Advances* **2014,** *4* (33), 17028-17038.

51. Larnaudie, S. C.; Brendel, J. C.; Romero-Canelón, I.; Sanchez-Cano, C.; Catrouillet, S.; Sanchis, J.; Coverdale, J. P. C.; Song, J.-I.; Habtemariam, A.; Sadler, P. J.; Jolliffe, K. A.; Perrier, S., Cyclic Peptide–Polymer Nanotubes as Efficient and Highly Potent Drug Delivery Systems for Organometallic Anticancer Complexes. *Biomacromolecules* **2018,** *19* (1), 239-247.

52. Pitkänen, L.; Tenkanen, M., Field-Flow Fractionation of Cationic Cellulose Derivatives. *Chromatographia* **2019,** *82* (12), 1827-1832.

53. Wyatt, P. J., Light scattering and the absolute characterization of macromolecules. *Analytica Chimica Acta* **1993,** *272* (1), 1-40.

54. Huglin, M. B., Determination of molecular weights by light scattering. In *Inorganic and Physical Chemistry*, Springer Berlin Heidelberg: Berlin, Heidelberg, 1978; Vol. 77, pp 141-232.

55. Panalytical, M. Principles of Triple Detection GPC/SEC. https://www.malvernpanalytical.com/en/learn/knowledge-center/whitepapers/wp151119principlestripledetectiongpc (accessed 23/06/2022).

56. Coto, B.; Escola, J. M.; Suárez, I.; Caballero, M. J., Determination of dn/dc values for ethylene–propylene copolymers. *Polymer Testing* **2007,** *26* (5), 568-575.

57. Wu, C. S., *Handbook Of Size Exclusion Chromatography And Related Techniques: Revised And Expanded*. 2nd ed.; Marcel Dekker: USA, 2003; Vol. 91.

58. Elias, H.-G., Scattering Methods. *Macromolecules* **2008**, 139-171.

59. Doncom, K. E. B.; Blackman, L. D.; Wright, D. B.; Gibson, M. I.; O'Reilly, R. K., Dispersity effects in polymer self-assemblies: a matter of hierarchical control. *Chemical Society Reviews* **2017,** *46* (14), 4119-4134.

60. Watterson, J. G.; Elias, H.-G., Characterization of Molecular Weight Distributions by the Standard Deviation. *Journal of Macromolecular Science: Part A - Chemistry* **1971,** *5* (2), 459-468.